

DNS OF TURBULENT FLOW OVER AN AXISYMMETRIC HILL

Jony Castagna

Faculty of Engineering,
Kingston UniversityRoehampton Vale, Friars Avenue, London, SW15 3DW, United Kingdom
k0543338@kingston.ac.uk

Yufeng Yao

Faculty of Engineering,
Kingston UniversityRoehampton Vale, Friars Avenue, London, SW15 3DW, United Kingdom
y.yao@kingston.ac.uk

ABSTRACT

Direct numerical simulation (DNS) of a turbulent flow over an axisymmetric hill has been carried out. The aim is to study three-dimensional flow separation and reattachment that occur on the lee-side of a curved geometry such as a hill shape. Simulation considers the flow conditions at Mach number of $M=0.6$ and the Reynolds number of $Re=500$, based on the free-stream quantities and the incoming boundary layer displacement thickness. The computational domain follows an existing wind tunnel test with the inlet distance adjusted for different inflow condition treatments. A total of three simulations are performed on the coarse and the fine grids, and a synthetic method is used for the generation of the inflow conditions. For coarse grids, simulations are carried out using both the synthetic method for inflow generation and the feed-in inflow data from a precursor computation. The results have shown good agreements between the two treatments, confirming the feasibility of using the feed-in inflow data technique. For fine grids, the resolutions are $\Delta x^+ = 12.5$, $\Delta z^+ = 6.5$, and $\Delta y_1^+ = 1.0$ with about 10 points in the viscous sublayer. Not surprisingly, further detailed flow structures and its development around the hill have been captured, which are quite different from those observed in the coarse grid simulations. It is found that a small separation bubble exists at the foot of the wind-side of the hill and the boundary layer flow laminarization occurs around the crest of the hill. These lead to different flow separation topologies in the lee-side of the hill, where a larger primary separation bubble embedded with a smaller secondary separations have been captured. Simulation results at this low Reynolds number could be used for future experimental validation studies.

INTRODUCTION

Three-dimensional flow separations can be found in many engineering flow applications, ranging from low-speed liquid flows to high-speed air flows. In order to understand the underlying flow separation mechanism, experimental and numerical studies have been carried out by many researches for flow over an obstacle, particularly the curved geometry. Despite of these efforts, our current understanding is still quite limited due to the complicity of this kind of flow separation (e.g. there is non-fixed separation points for flow over a curved-body). Furthermore, the flow contains some complicated three-dimensional separation topologies and of-

ten associated with high-level of unsteadiness. These will cause certain difficulties for accurate experimental measurements of the near wall flow properties. Recent advancement in computing power and numerical algorithm has made it possible to study this kind of complex flow by numerical computations and the direct numerical simulation (DNS) is an ideal methodology, in which the spacial and the temporal development of the turbulent flow can be simulated without intervene *ad hoc* turbulence models.

The problem of turbulent flow over an axisymmetric hill was originally proposed and experimentally studied by Simpson et al. (2002) at a high Reynolds number of 1.3×10^5 , based on the free-stream quantities and the hill height. Later, numerous numerical investigations have been carried out by various modeling approaches, e.g. URANS and LES (Tessicini et al., 2007, Patel et al., 2007, and Wang et al., 2004) at either full or reduced experimental Reynolds number. To author's knowledge, there is no published work on DNS of the hill flow, simply because of the high Reynolds number requires huge amount of computer resources that is difficult to meet even with the current HPC resource. However, simulation at a reduced Reynolds number (Patel et al. 2007) is feasible and the results are also valuable to enhance our current understanding on this complex flow configuration. Hence, this study considers simulations at $Re_{\delta^*} = 500$ (i.e. 1/20 of the experimental condition) and results will be compared qualitatively with those from the high-Re experiment. The low Reynolds number used in simulation will lead to a thicker boundary layer, thus increases the possibility of flow re-laminarization, particularly in the favorite pressure gradient region, i.e. the wind-side of the hill. If it happens, it will have influences on the downstream flow separations, which are the most important feature in the hill flow.

In the simulation of a spatial-developing turbulent flow, particular attentions are required on the quality of the inlet condition (Tessicini et al., 2007). For the hill flow simulation, the inflow profile is influential on the simulation results as discussed by Li et al. (2005). It was concluded that given the upstream turbulent mean velocity profile agreed well with the experimental data, any uncorrelated fluctuations introduced will still lead to the inaccurate development of the boundary layer over the hill. Thus, in order to ensure the good quality of inflow data at given conditions, a separate precursor computation of a zero-pressure gradient turbulent boundary layer is often used and validated against the benchmark results. Then time sequence of instantaneous

flow data can be stored for the follow-up main simulations.

In this study, two inflow treatments are considered, one with the feed-in data from a precursor simulation and the other with the embedded inflow generator. Comparison of two approaches will be made to validate the proposed data feed-in technique. Simulation considers the Mach number of $M=0.6$ and the Reynolds number of 500; the former can permit larger time step for simulation using the compressible solver and the latter will significantly reduce the required computer resources. The Mach number effect has been studied previously by Cui et al. (2003) on a channel flow configuration and it was concluded that the compressibility effect is not very significant on the results. Simulation results at the low-Re will be compared with the high-Re experiment qualitatively such as the flow topologies. Some quantitative turbulence properties will be presented as well.

GOVERNING EQUATIONS AND THE FLOW SOLVER

The non-dimensional form of three-dimensional compressible Navier-Stokes equation in the Cartesian coordinate system can be written as

$$\frac{\partial \rho}{\partial t} + \frac{\partial(\rho u_i)}{\partial x_i} = 0 \quad (1)$$

$$\frac{\partial(\rho u_i)}{\partial t} + \frac{\partial(\rho u_i u_j)}{\partial x_j} = -\frac{\partial p}{\partial x_i} + \frac{1}{Re} \frac{\partial \tau_{ij}}{\partial x_j} \quad (2)$$

$$\begin{aligned} \frac{\partial E}{\partial t} + \frac{\partial[(E+p)u_j]}{\partial x_j} = \\ -\frac{1}{(\gamma-1)RePrM^2} \frac{\partial}{\partial x_j} \left(\mu \frac{\partial T}{\partial x_j} \right) + \frac{1}{Re} \frac{\partial u_j \tau_{ij}}{\partial x_i} \end{aligned} \quad (3)$$

where x_i, x_j are the Cartesian coordinates, t is the time variable. The free-stream quantities are used for the dimensionalization and the non-dimensional physical variables are ρ the density, u_i, u_j the velocity components, p the pressure, T the temperature, and E the total energy. The τ_{ij} is the shear stress tensor, μ the dynamic viscosity (calculated by using the power law $\mu = T^\omega$ with $\omega = 0.76$), Re the Reynolds number (defined as $Re_{\delta^*} = \rho_\infty u_\infty \delta^* / \mu_\infty$, where δ^* is the inflow boundary layer displacement thickness), Pr the Prandtl number and M the Mach number (defined as $M = u_\infty / c_\infty$, where c_∞ is the free-stream sound speed), respectively.

An in-house DNS solver (SBLI) is used in this study. The code uses the high-order finite difference technique with the curvilinear body-fitted grids in the Cartesian coordinate system for curved geometry treatment. The spatial derivatives (both convective and diffusion terms) are approximated by using the 4th-order central scheme for the interior grid points and a stable high-order boundary scheme based on the summation by parts (SBP) approach of Carpenter et al. (1999) for the boundary grid points. A three-step compact Runge-Kutta algorithm is used for the time integration. For shock capturing, the TVD scheme is applied. One unique feature of this code is the application of the entropy splitting concept (Sandham, et al. 2002) to improve numerical stability, which is very important for a DNS solver that often requires extremely longer run time to achieve the statistically converged results. The code has been parallelized using the MPI library with very good scalability performance at various high-performance computing platforms. The code has been re-engineered recently with comprehensive verification

and validation studies. More details can be found in Yao et al. (2009).

PROBLEM DEFINITION AND BOUNDARY CONDITIONS

Figure 1 gives the sketch of the hill flow configuration, where H is the hill height, and L_x, L_y, L_z are dimensions of the computational domain.

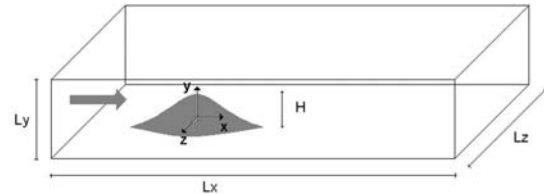


Figure 1: Sketch of the hill flow configuration.

The hill shape is defined as (Simpson et al. 2002)

$$\frac{y(r)}{H} = -\beta[\mathbf{J}_0(\Lambda)\mathbf{I}_0(r\Lambda/a) - \mathbf{I}_0(\Lambda)\mathbf{J}_0(r\Lambda/a)] \quad (4)$$

where $y(r)$ is the shape function of the radius r . The coefficients are $\beta=1/6.048$, $\Lambda=3.1926$, $a=2H$. The \mathbf{J}_0 and \mathbf{I}_0 are the Bessel and modified Bessel functions, respectively. This defines a hill geometry of H in height at the center and $2H$ in radius at the ground surface.

The center of the hill is at $4.4H$ from the inlet plane for simulation with the feed-in inflow data from a precursor simulation, and this distance is increased to $8.4H$ for simulation without using the precursor inflow data. The distance between the center of the hill and the domain outlet is fixed as $11.6H$, resulting in the streamwise domain length of $L_x = 16H$ or $L_x = 20H$ for simulations with and without the precursor inflow data. The domain height is fixed as $L_y = 2.305H$ and the domain width $L_z = 8.62H$ which is wider enough to have a wide range of turbulent fluctuations frequencies.

The boundary conditions are defined as follows: a no-slip condition for the wall and the hill surfaces; a fully-developed turbulent boundary layer at inlet plane (either by the feed-in precursor inflow data or by synthetic method embedded in the simulation); a non-reflecting characteristic condition at the outlet and upper surfaces; and periodic condition for side walls in the spanwise direction.

The inflow condition is generated by using the synthesis method (Klein et al. 2003) either embedded into the hill flow simulation or used for a separate precursor boundary layer simulation then applying the data feed-in technique for the main hill flow simulation as described in the next section.

TURBULENT BOUNDARY LAYER SIMULATION

A precursor turbulent boundary layer flow simulation at the same flow conditions as those for the hill flow simulation is carried out to generate the inlet conditions. The precursor simulation domain is $50\delta^*$, $10\delta^*$ and $8\delta^*$ in the streamwise (x), the wall normal (y) and the spanwise (z) directions, where the δ^* is the displacement thickness of the boundary layer at the inlet. A grid of $119 \times 61 \times 71$ points is used, uniformly distributed in the x, z directions and stretched in the y direction. Based on the inflow conditions, the estimated grid resolutions are $\Delta x^+ = 11.09$, $\Delta z^+ = 6.24$ and the first point in the wall normal direction is about $\Delta y_1^+ = 0.99$ with a total of 10 points in the viscous sublayer region. To reduce the computational time, the precursor simulation is

normally using a narrow domain ($Lz = 8\delta^*$ in this case), but large enough for the development of the boundary layer. A two-point correlation is often used to find out the minimum width required for the computation and this has been confirmed in present simulations.

A synthetic approach of the digital filter technique (Klein et al. 2003) has been used. In this method, turbulent boundary layer properties (both the mean velocity and the Reynolds stress profiles) are prescribed, along with artificially generated random numbers as white noise. A filter procedure is then used to retain the appropriate values to reproduce the desirable turbulent correlations for given conditions.

The precursor simulation starts with a uniform flow field and after initial transient stage of about 100 time units (i.e. two through flows), statistic samples are collected for every 100 time units until the 'statistical' convergence achieved. This normally takes about 400 time units (i.e. 8 through flows).

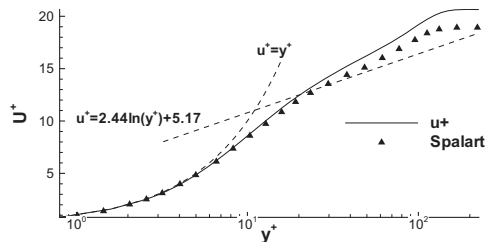


Figure 2: Mean streamwise velocity U^+ at $x/\delta^* = 45$.

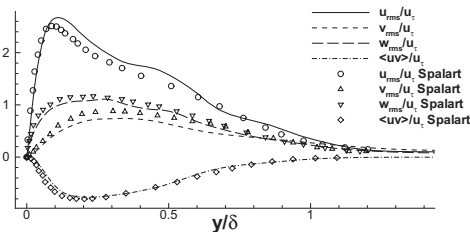


Figure 3: Turbulence intensities at $x/\delta^* = 45$.

The mean velocity U^+ , the RMS of the turbulence intensities (u_{rms} , v_{rms} , w_{rms}) and the Reynolds stress ($\langle uv \rangle$) variations are shown in Figures 2 and 3, where y^+ is the y -coordinate in the wall unit and δ is the boundary layer thickness and the variables are normalized by the friction velocity u_τ . The results are compared with the benchmark DNS data of Spalart (1988) at the same Reynolds number. It can be seen that the overall agreements are quite good, with slightly over-prediction in the wake region of the mean velocity profile and the streamwise turbulence intensity u_{rms} .

The simulation results at $x/\delta^* \simeq 45$ are saved at every 5-iteration intervals. This will result in a time sequence of two-dimensional instantaneous flow at a cross-section. In general, the precursor simulation has smaller cross-section, and the data needs to be manipulated by copying onto the inlet plane of the main simulation domain. The uniform free-stream conditions are applied for the region above the upper surface of the precursor simulation (i.e. $y > 10\delta^*$ in present study). During the simulation, the time interpolations are also required. Figure 4 gives the diagram of the interface between the precursor simulation and the main simulation.

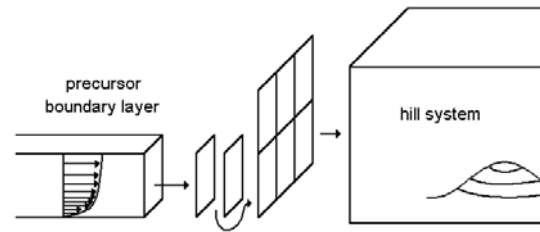


Figure 4: Diagram of interface of precursor-hill simulation.

TURBULENT FLOW OVER THE HILL

Simulations of a turbulent flow over the hill have been carried out with three cases; test *I* with the embedded inflow conditions generation in the simulation, test *II* with the feed-in inflow conditions from a precursor simulation, and test *III* with the feed-in inflow data but on fine grids. The grid resolution for all three tests is given in Table 1:

Table 1: Resolution of test cases.

test	N_x, N_y, N_z	Δx^+	Δy^+	Δz^+
I	128,70,120	57.06	11.26~28.72	26.22
II	120,70,120	48.69	11.26~28.72	26.22
III	480,160,480	12.17	1.06~25.37	6.55

The estimations are based on the prescribed inflow profile. For tests *I* and *II*, simulations are under-resolved by a factor of 4 in both the streamwise and spanwise directions and the first grid point is just above the sublayer. In contrary, test *III* has good grid resolutions in the streamwise and spanwise directions and there are about 8~10 points in the viscous sublayer.

The inflow boundary layer thickness is about $6.5\delta^*$, based on the precursor simulation. For the hill simulation, the hill height H is roughly about 2δ , i.e. $H = 13.0\delta^*$. This leads to the simulation Reynolds number based on the hill height H about $Re_H \simeq 6500$, about 1/20 of the experiment Reynolds number.

Coarse grid results

Two coarse grids tests are carried out; test *I* runs with an extended inflow domain with the synthetic method used at the inlet and test *II* uses the feed-in flow data from a precursor simulation as inflow conditions at the inlet. For both cases, after initial transient runs of about 300 time units, statistics data are collected for further 900 time units. Figure 5 gives the comparison of the separation bubble boundary. It can be seen that results from two tests agree well and small wiggles observed near the reattachment region are likely associated with the coarse grid resolution. This confirms that the feed-in technique works well and the same method will be used for the fine grid test *III* described later.

Figure 6 shows the contours of the pressure coefficient C_p on the wall surface. It can be seen that the C_p increases at the wind-side of the hill and decreases at the lee-side of the hill. Downstream in the wake region, the pressure recovers. The predicted minimum C_p happens around the top of the hill and, after about $x/H = 2$, it increases again with higher value in central area downstream of the hill. These features are in qualitatively good agreement with those observed by Simpson et al. (2002) in the high-Re experiments.

The lee-side flow separation bubble can be seen in Figure

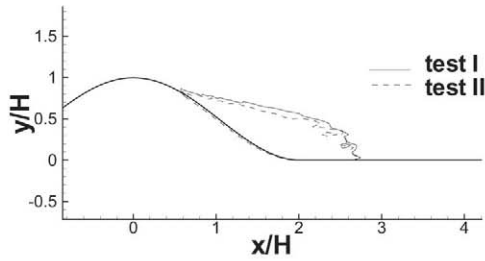


Figure 5: Comparison of separation bubble boundary between tests *I* and *II*.

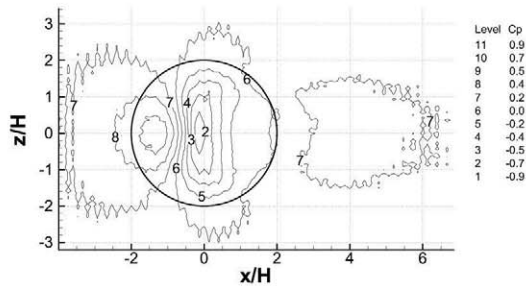


Figure 6: Contours of pressure coefficient on the wall surface.

7, where the streamlines illustrate the flow re-circulation at the mid-plane $z = 0$. In this plane, the separation starts about $x/H = 0.5$ with a small closed bubble, followed by a more dominant large bubble with its center at about $x/H = 2, y/H = 0.5$. The flow reattaches at about $x/H = 2.75$. In the high-Re experiment, a small recirculation zone enclosing a very thin and elongated strip attached to the lee-side of the hill was observed. In comparison, the predicted bubble size is much larger, and this is probably due to the Reynolds number effects.

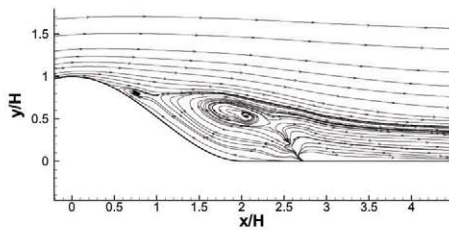


Figure 7: Streamlines in the central plane of $z=0$.

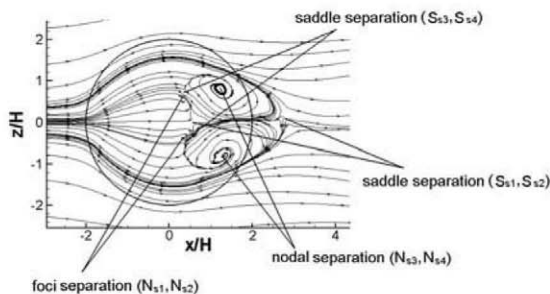


Figure 8: Flow topologies in the near wall at $y^+=11.26$.

Figure 8 illustrates the three-dimensional flow separations with the counter rotating vortex pair (CRVP) being captured on the lee-side of the hill. The topology analysis of

flow separation and reattachment is also shown in this figure, where two saddle points (S_{s1} and S_{s2}) are identified at $x/H=0.52$, and $x/H=2.8$, at the mid-plane of $z/H=0$; along with two nodal foci points (N_{n1} and N_{n2}) at $x/H=0.34, z/H=\pm 0.61$; two further nodal points (N_{n3} and N_{n4}) at $x/H=1.31, y/H=0.17, z/H=\pm 0.8$ (i.e. the center of vortex core at the hill surface), and two further saddle points (S_{s3} and S_{s4}) at $x/H=0.34, z/H=\pm 0.72$. In the high-Re experiment, only one pair of nodal and saddle separation points were identified. Here, two pairs of nodal and saddle separation points are captured in the low-Re simulation. The topology satisfies the well-defined rule (Hunt et al. 2006) as

$$\sum N - \sum S = 0 \quad (5)$$

where N and S are the number of nodal and saddle points, respectively.

Fine grid results

The fine grid test *III* adopts the feed-in inflow data for precursor simulation. After initial transient stage, statistic data are collected for a time period of 400 time units, with the convergence being verified and confirmed, though the duration is shorter than that of coarse grid simulation.

The mean streamwise velocity profile U^+ is shown in Figure 9. The boundary layer thickness is about $=6.9\delta^*$ at the inlet plane $x/H = -4.4$, slightly larger than that from precursor simulation. Different from the coarse grid, simulation on fine grid predicts a small separation bubble at the foot of the wind-side of the hill at $x/H = -2$, this causes the rapid reduction of the friction velocity at $x/H = -3$ by almost half of the inflow value. Hence the mean velocity in the wall unit has been doubled in the edge of the boundary layer. At $x/H = -1$, the friction velocity recovers and increases, leading to a lower U^+ value there.

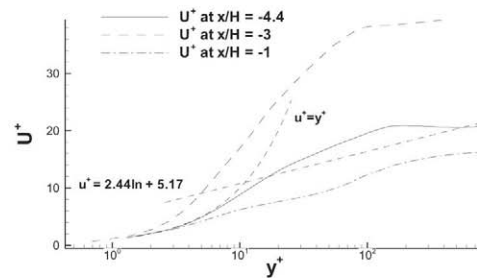


Figure 9: Mean streamwise velocity U^+ at the inlet plane.

Figure 10 gives the streamlines from the fine grid simulation. Comparing to that of coarse grid, the separation bubble increases in size. The flow separation starts earlier at the crest of the hill and reattaches later at about $x/H \simeq 4$. The re-circulation center is about $x/H = 2.1, y/H = 1.0$. The improved grid resolution permits the simulation to capture a small secondary re-circulation bubble embedded inside the primary re-circulation bubble. The streamline plot also reveals a small separation (not shown here) occurring at the foot of the hill $x/H = -2$. This bubble, although very small in size, seems to have some considerable influence on the flow separation behavior.

The three-dimensional flow separation can be found from the streamline patterns in the near wall region as seen in Figure 11. As before the counter-rotating vortex pair exists. The flow topology analysis have identified three saddle separation points S_{s1}, S_{s2} and S_{s3} along the mid-plane ($z=0$)

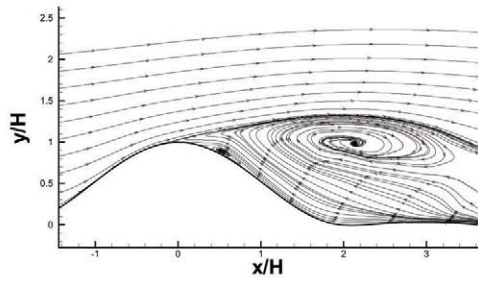


Figure 10: Streamline in the x - y central plane ($z=0$).

at $x/H=-2.4$, $x/H=-0.1$ and $x/H=4$, and three nodal separation points N_{s1} , N_{s2} and N_{s3} at $x/H=-1.6$, $z/H=0$ and $x/H=1.3$, $z/H=\pm 0.8$. Same as before, they satisfy the rule defined by Eq. (6).

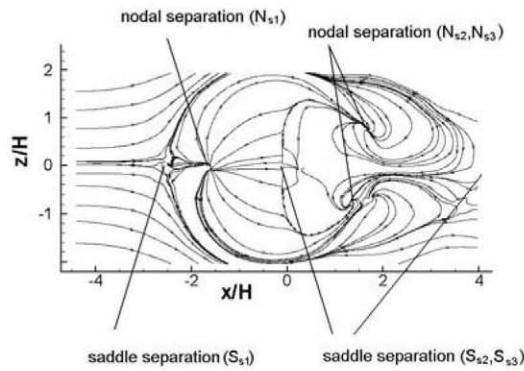


Figure 11: Flow topologies in the near wall at $y^+ = 1.06$.

Figures 12-14 gives the RMS turbulent intensities and the Reynolds stress (normalized by the friction velocity u_τ) at three successively streamwise locations of $x/H = -4.4, -3, -1$, respectively. At the inlet ($x=-4.4$), the predictions are in good agreement with the DNS of Spalart (1988), indicating the feed-in inflow data technique also work well on the fine grid. Downstream at $x/H = -3$, the RMS quantities and the Reynolds stress are over-predicted about a factor of 2 compared to the Spalart data, in consistent with that seen in Figure 9. The reason for this is probably due to the rapid decrease of the friction velocity, as a result of the presence of a small separation bubble at $x/H = -2$. At $x/H = -1$ before the crest of the hill, the normalized RMS decreases (due to increases of friction velocity), but quite surprisingly, the Reynolds stress has shown a 'positive' peak value of about 1.8. Further analysis on the budgets balance is necessary to understand the cause of this.

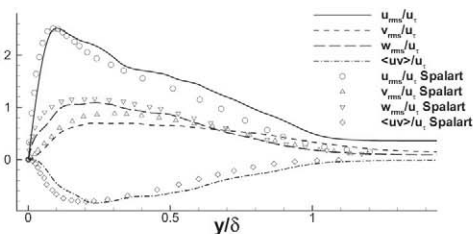


Figure 12: Turbulent intensity and Reynolds stress at $x/H=-4.4$.

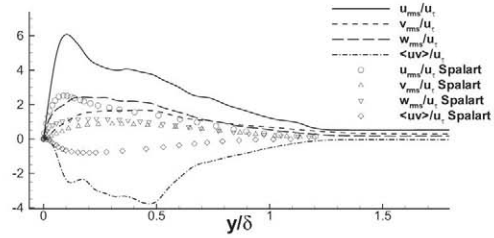


Figure 13: Turbulent intensity and Reynolds stress at $x/H=-3$.

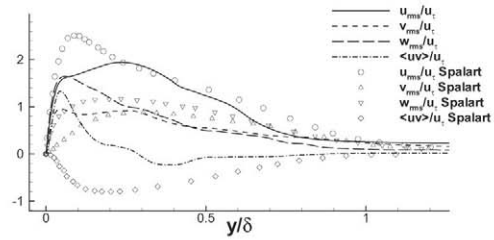


Figure 14: Turbulent intensity and Reynolds stress at $x/H=-1$.

Turbulent flow structures

Figure 15 gives the fine grid flow structures illustrated with the iso-surfaces of the second invariants $\lambda_2 = 0.035$ of the symmetric tensor of instantaneous velocity flow field (Jeong and Hussain, 2006). Similarly, Figure 16 shows the coarse grid flow structures at the same value of $\lambda_2 = 0.035$. For fine grid, it can be seen that the flow structures occurs in a larger area in the lee-side of the hill (consistent with larger separation bubble), but they are rarely seen around the top of the hill. This indicates the flow may be partly re-laminarized in that region. For coarse grid, the flow structures still exist around the crest of the hill.

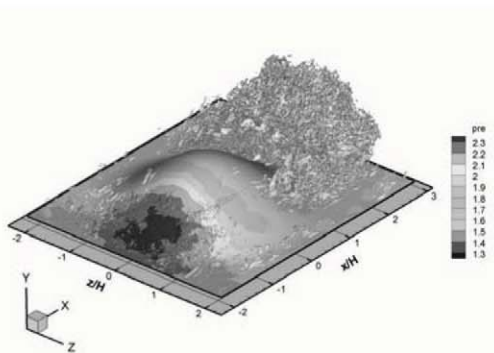


Figure 15: Flow structures at $\lambda_2=0.035$ from fine grid simulation.

Re-laminarization issue

Due to low-Re used in the simulation and strong favorable pressure gradient at the wind-side of the hill, the laminarization may occur. In a previous study by Sandham et al. (2003) for a turbulent flow over a bump geometry, the flow re-laminarization issue has been studied by using a criteria related to a general acceleration parameter (Jones and Launder, 1972) as

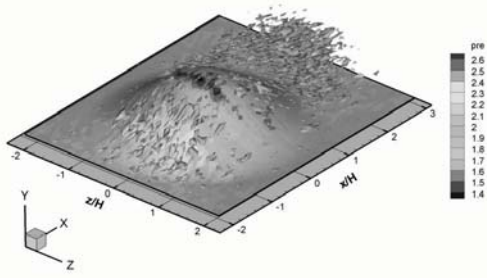


Figure 16: Flow structures at $\lambda_2=0.035$ from coarse grid simulation.

$$K = \frac{\nu_e}{U_e^2} \frac{\partial U_e}{\partial x} \quad (6)$$

where the 'e' represents the boundary layer edge and the criterion for flow laminarization occurs roughly at $K > 3 \times 10^{-6}$. For present hill simulation, the K variation is evaluated at the top boundary of the domain (i.e. $y = 3.205H$). The results shown in Figure 17) confirms that the K value has indeed exceeded the given criteria for laminarization. It is believed that the flow laminarization contributes to the larger separation bubble seen in Figure 10.

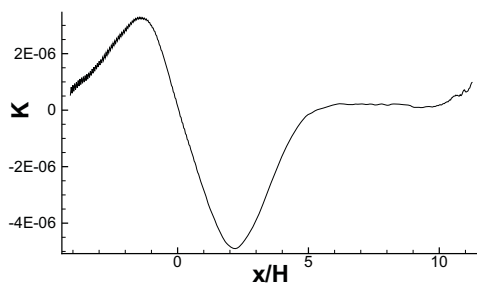


Figure 17: Laminarization parameter K variations at $y = 3.205H$.

CONCLUSION

Direct numerical simulation of a turbulent flow over an axisymmetric hill shape is performed. Simulation considers a low Reynolds number 500, which is about 1/20 of the experiment condition. Despite this difference, simulations are still able to capture the dynamic flow behavior and the key flow topologies in the separation region, in good qualitative agreement with the high-Re test. However, the predicted flow separation bubble at present low-Re seems much larger in size compared to that observed in the high-Re experiment. The simulation also reveals a small separation at the wind-side of the hill near the foot and a secondary separation bubble embedded inside a primary large bubble at the lee-side of the hill. It is found that the flow laminarization occurs in the vicinity of the crest of the hill. Consequently, this will alter the flow development and contribute to the earlier flow separation and the larger bubble. These findings are useful for future experimental validation study at low Reynolds number.

ACKNOWLEDGEMENT

The first author would like to acknowledge the finance support from the Kingston University, London and the computational time resource is supported by the UK Turbulence Consortia under the EPSRC grant (EP/D044073/1).

REFERENCES

- Carpenter M.H., Nordstrom J., and Gottlieb D., 1999, "A Stable and Conservative Interface Treatment of Arbitrary Spatial Accuracy", *Journal of Computational Physics*, Vol. 148(2), pp. 341-365.
- Cui, J., Patel, V.C., and Lin, C.L., 2003, "Large-eddy simulation of turbulent flow in a channel with rib roughness", *International Journal of Heat and Fluid Flow*, Vol. 24(3), pp. 372-388.
- Hunt, J.C.R., Abell, C.J., Peterka, J.A., and Woo, H., 2006, "Kinematical studies of the flows around free or surface-mounted obstacles; applying topology to flow visualization", *Journal of Fluid Mechanics*, Vol. 86(01), pp. 179-200.
- Jeong, J., and Hussain, F., 2006, "On the identification of a vortex", *Journal of Fluid Mechanics*, Vol. 285, pp. 69-94.
- Jones, W.P., and Launder, B.E., 1972, "The prediction of laminarization with a two-equation model of turbulence", *International Journal of Heat and Mass Transfer*, Vol. 15, pp. 301-314.
- Klein, M., Sadiki, A., and Janicka, J., 2003, "A digital filter based generation of inflow data for spatially developing direct numerical or large eddy simulations", *Journal of Computational Physics*, Vol. 186(2), pp. 652-665.
- Li, N., Wang, C., Avdis, A., Leschziner M.A., and Temmerman, L., 2005, "Large eddy simulation of separation from a three-dimensional hill versus second-moment-closure RANS modelling", *Proceedings of the Fourth Int. Symp. on Turbulence and Shear Flow Phenomena (TSFP4)*, pp. 331-336.
- Patel, N., and Menon, S., 2007, "Structure of flow separation and reattachment behind an axisymmetric hill", *Int. Journal of Heat and Fluid Flow*, Vol. 24(3), pp. 372-388.
- Sandham, N.D., Li, Q., and Yee, H.C., 2002, "Entropy splitting for high-order numerical simulation of compressible turbulence", *Journal of Computational Physics*, Vol. 178(2), pp. 307-322.
- Sandham, N.D., Yao, Y.F., and Lawal, 2003, "Large-eddy simulation of transonic turbulent flow over a bump", *International Journal of Heat and Fluid Flow*, Vol. 24(4), pp. 584-595.
- Spalart, P.R., 1988, "Direct simulation of a turbulent boundary layer up to $Re_\theta = 1410$ ", *Journal of Fluid Mechanics*, Vol. 187, pp. 61-98.
- Simpson, R.L., Long, C.H., and Byun, G. 2002, "Study of vortical separation from an axisymmetric hill", *International Journal of Heat and Fluid Flow*, Vol. 23(5), pp. 582-591.
- Tessicini, F., Li, N., and Leschziner, M.A. 2007, "Large-eddy simulation of three-dimensional flow around a hill-shaped obstruction with a zonal near-wall approximation", *Int. Journal of Heat and Fluid Flow*, Vol. 28(5), pp. 894-908.
- Wang, C., Jang, Y.J., and Leschziner, M.A., 2004, "Modelling two- and three-dimensional separation from curved surfaces with anisotropy-resolving turbulence closures" *Int. Journal of Heat and Fluid Flow*, Vol. 25(3), pp. 499-512.
- Yao, Y.F., et al., 2009, "To re-engineer a DNS code for high-performance computation of turbulent flow simulation", AIAA 2009-0566, Orlando, FL, USA.